AMERICAN SOCIETY FOR MICROBIOLOGY | Journal of Virology®

GENOME REPLICATION AND REGULATION OF VIRAL GENE EXPRESSION

A Stem-Loop Structure in *Potato Leafroll Virus* Open Reading Frame 5 (ORF5) Is Essential for Readthrough Translation of the Coat Protein ORF Stop Codon 700 Bases Upstream

Yi Xu,[a] Ho-Jong Ju,[a]* Stacy DeBlasio,[b] Elizabeth J. Carino,[c] Richard Johnson,[d] Michael J. MacCoss,[d] Michelle Heck,[b,e] W. Allen Miller,[c] Stewart M. Gray[a,b]

[a]Section of Plant Pathology and Plant-Microbe Biology, School of Integrated Plant Science, Cornell University, Ithaca, New York, USA

[b]Emerging Pests and Pathogens Research Unit, USDA, ARS, Ithaca, New York, USA

[c]Department of Plant Pathology and Microbiology, Iowa State University, Ames, Iowa, USA

[d]Department of Genome Sciences, University of Washington, Seattle, Washington, USA

[e]Boyce Thompson Institute, Ithaca, New York, USA

ABSTRACT Translational readthrough of the stop codon of the capsid protein (CP) open reading frame (ORF) is used by members of the *Luteoviridae* to produce their minor capsid protein as a readthrough protein (RTP). The elements regulating RTP expression are not well understood, but they involve long-distance interactions between RNA domains. Using high-resolution mass spectrometry, glutamine and tyrosine were identified as the primary amino acids inserted at the stop codon of *Potato leafroll virus* (PLRV) CP ORF. We characterized the contributions of a cytidine-rich domain immediately downstream and a branched stem-loop structure 600 to 700 nucleotides downstream of the CP stop codon. Mutations predicted to disrupt and restore the base of the distal stem-loop structure prevented and restored stop codon readthrough. Motifs in the downstream readthrough element (DRTE) are predicted to base pair to a site within 27 nucleotides (nt) of the CP ORF stop codon. Consistent with a requirement for this base pairing, the DRTE of *Cereal yellow dwarf virus* was not compatible with the stop codon-proximal element of PLRV in facilitating readthrough. Moreover, deletion of the complementary tract of bases from the stop codon-proximal region or the DRTE of PLRV prevented readthrough. In contrast, the distance and sequence composition between the two domains was flexible. Mutants deficient in RTP translation moved long distances in plants, but fewer infection foci developed in systemically infected leaves. Selective 2′-hydroxyl acylation and primer extension (SHAPE) probing to determine the secondary structure of the mutant DRTEs revealed that the functional mutants were more likely to have bases accessible for long-distance base pairing than the nonfunctional mutants. This study reveals a heretofore unknown combination of RNA structure and sequence that reduces stop codon efficiency, allowing translation of a key viral protein.

IMPORTANCE Programmed stop codon readthrough is used by many animal and plant viruses to produce key viral proteins. Moreover, such "leaky" stop codons are used in host mRNAs or can arise from mutations that cause genetic disease. Thus, it is important to understand the mechanism(s) of stop codon readthrough. Here, we shed light on the mechanism of readthrough of the stop codon of the coat protein ORFs of viruses in the *Luteoviridae* by identifying the amino acids inserted at the stop codon and RNA structures that facilitate this "leakiness" of the stop codon. Members of the *Luteoviridae* encode a C-terminal extension to the capsid protein known as the readthrough protein (RTP). We characterized two RNA domains in *Potato leafroll virus* (PLRV), located 600 to 700 nucleotides apart, that are essential for

Received 1 September 2017 **Accepted** 6 March 2018

Accepted manuscript posted online 7 March 2018

Citation Xu Y, Ju H-J, DeBlasio S, Carino EJ, Johnson R, MacCoss MJ, Heck M, Miller WA, Gray SM. 2018. A stem-loop structure in *Potato leafroll virus* open reading frame 5 (ORF5) is essential for readthrough translation of the coat protein ORF stop codon 700 bases upstream. J Virol 92:e01544-17. https://doi.org/10.1128/JVI.01544-17.

Editor Anne E. Simon, University of Maryland, College Park

Address correspondence to W. Allen Miller, wamiller@iastate.edu, or Stewart M. Gray, smg3@cornell.edu.

* Present address: Ho-Jong Ju, Department of Agricultural Biology, College of Agriculture & Life Sciences, Chonbuk National University, Jeonju-si, Republic of Korea.

efficient RTP translation. We further determined that the PLRV readthrough process involves both local structures and long-range RNA-RNA interactions. Genetic manipulation of the RNA structure altered the ability of PLRV to translate RTP and systemically infect the plant. This demonstrates that plant virus RNA contains multiple layers of information beyond the primary sequence and extends our understanding of stop codon readthrough. Strategic targets that can be exploited to disrupt the virus life cycle and reduce its ability to move within and between plant hosts were revealed.

KEYWORDS RNA structure, polerovirus, readthrough, systemic infection, translational control

Translational readthrough of a stop codon is an evolutionarily conserved event that many viruses have adopted to increase the number of expressed viral proteins while maintaining a compact genome size (1–4). It is also a strategy that has recently been recognized in several eukaryotic organisms (5). Normally, termination of translation in eukaryotes at a stop codon is a highly efficient process that requires the collective action of two release factors, eRF1 and eRF3 (6, 7). While eRF1, a structural mimic of an A-site tRNA, binds to and recognizes all three stop codons (UAA, UAG, and UGA), the formation of an eRF1-eRF3 complex and the eRF3-associated GTPase activity are required for termination of translation (8). The type of stop codon present and its flanking nucleotides, as well as other distal elements, can influence termination efficiency (4, 9–11).

In translational readthrough, the stop codon is misread as a sense codon and decoded by a near cognate or suppressor tRNA, allowing translation to continue to the next termination codon. Programmed translational readthrough allows the production of a C-terminal extended polypeptide at a defined frequency (1). Long-range communication between structural features of RNA can regulate readthrough translation efficiency and is a common feature of several plant viruses (4, 12, 13). Most of that work focused on readthrough translation of replication-associated proteins that is facilitated by distal elements located in the 3′ untranslated region (UTR).

In contrast to the expression of replication proteins via readthrough, all members of the *Luteoviridae* (collectively referred to as luteovirids) rely on this mechanism to express their minor capsid protein. These viruses have a nonenveloped, spherical virion about 23 nm in diameter with T=3 icosahedral symmetry and composed of 180 capsid protein monomers. Most of the 180 monomers are the major 22- to 25-kDa capsid protein (CP), but a small percentage contain a long C-terminal extension, which is translated via stop codon readthrough. The extension appears to be located on the virion surface (14–16). The readthrough proteins (RTP) of several luteovirids, comprising the open reading frame 3 (ORF3)-encoded CP and the ORF5-encoded readthrough domain (RTD) (approximately 56 kDa), have been studied extensively (15, 17–20). The full-length RTP (80 kDa) is detected readily in infected plant tissues, but in purified virus preparations, a significant portion of the C terminus of the RTD is proteolytically processed, yielding a 51- to 58-kDa RTP (15, 17–20). The RTD contains a highly conserved N-terminal region and a variable C-terminal region (21). The N terminus of the RTD mediates RTP incorporation into the virion and is required for aphid transmission (17, 22–24). The variable RTD C-terminal domain is not required for transmission, but it does appear to enhance aphid transmission efficiency (19). This domain also functions in phloem retention of the virus (25) and influences systemic infection, virus accumulation, and symptom development (17, 20, 26, 27).

Other plant viruses, including the pomoviruses, benyviruses, and furoviruses, also use translational readthrough of the CP stop codon to produce minor capsid proteins (28, 29), some of which have been shown to have functions similar to those of the *Potato leafroll virus* (PLRV) RTP. The RTP of potato mop-top virus, the type species of the genus *Pomovirus*, is essential for transmission by its protist vector and for systemic movement of viral RNAs (28, 30). Although the mechanisms of readthrough translation of the minor capsid proteins of the pomoviruses, benyviruses, and furoviruses are not

well studied, Firth et al. identified conserved 3′ stem-loop structures in these viruses that are similar to those involved in alphavirus readthrough stimulation (10).

Readthrough of the *Barley yellow dwarf virus* PAV (BYDV-PAV) (*Luteovirus*, *Luteoviridae*) ORF3 stop codon requires two essential RNA domains downstream: a series of CCN-NNN repeats starting seven bases downstream of the stop codon and another sequence located 700 nucleotides (nt) downstream (11). For PLRV, Tacke et al. found that a sequence containing 18 nt before and 21 nt after the CP stop resulted in only 0.9 to 1.3% readthrough translation relative to the wild-type (WT) level in tobacco and potato protoplasts (31), indicating that there may be some other elements required for PLRV CP stop codon readthrough. The mechanisms associated with RTD translation were not characterized for PLRV. Here we identified and characterized two RNA domains in ORF5 of PLRV that affect RTP translation efficiency: a cytidine-rich (C-rich) domain and a complex stem-loop structure located adjacent to and 640 nucleotides downstream of the CP stop codon. Communication between the two domains was virus specific and indispensable for RTP translation. Additionally, the distal domain is under selection to maintain a highly base-paired structure that ensures efficient translational readthrough.

RESULTS

Identification of the amino acids incorporated at the leaky UAG coat protein stop codon. In translational readthrough events studied to date, readthrough is achieved by misreading of termination codons by endogenous tRNAs whose structure and intrinsic features contribute to the ability to read noncognate codons (1, 32). To identify the inserted amino acid at the site of the leaky UAG codon in PLRV RNA and better understand whether readthrough of the PLRV CP stop codon favors a specific aminoacylated tRNA, virus structural proteins were affinity purified from locally infected *Nicotiana benthamiana* sap and analyzed using high-resolution mass spectrometry. A set of triply charged PLRV RTP peptides with the consensus sequence K.X_{209}VDSGSEP GPSPQPTPTPTPQKHER.F were identified, with precursor ion mass/charge ratios (*m/z*) indicating the amino acid glutamine (Q), tyrosine (Y), or histidine (H) at the 209 position of the CP amber stop codon (Fig. 1A to C). Peptide sequence identity was confirmed by manual verification of the tandem mass spectra (MS^2) associated with each peptide (Fig. 1A to C). As expected, all y fragment ions detected had similar *m/z* values, indicating that the three peptides share the same amino acid composition downstream of the CP amber stop codon (first peptide position), with peptide K.Y_{209}VDSGSEPGPS PQPTPTPTPQKHER.F being deamidated at position Q_{229}. However, higher-order b ions in each spectrum, relative to the other two, exhibited mass shifts corresponding to the known mass differences between residues Q, H, and Y being incorporated at the site of the amber stop codon. The spectrum associated with peptide K.Y_{209}VDSGSEPGPSPQP TPTPTPQKHER.F also exhibited an intense peak at *m/z* 136.067 (Fig. 1C), which is indicative of the immonium ion of tyrosine, further confirming the identity of the CP stop codon residue in this peptide, since no other Y residues are present in the remainder of the peptide sequence. Comparison of MS1 peak areas for the corresponding precursor ions of each peptide, a measure of their relative abundance, indicated that ~89% and ~10% of the K.X_{209}VDSGSEPGPSPQPTPTPTPQKHER.F peptides had Q and Y, respectively, at position 209 (Fig. 1D). Fewer than 1% of the peptides contained an H (Fig. 1D). These results are consistent with previous findings that plant cytoplasmic $tRNA^{Tyr}$ and $tRNA^{Gln}$ can be incorporated at the UAG codon by tRNAs (1).

Identification of the distal element responsible for RTP expression. To determine the mechanisms regulating the translational readthrough of the PLRV CP stop codon, a series of deletion and point mutations were constructed in ORF5 of a PLRV infectious cDNA clone as described previously (33) (Fig. 2A). Double-antibody sandwich enzyme-linked immunosorbent assay (DAS-ELISA) analysis of *N. benthamiana* leaves agroinfiltrated with wild-type PLRV and various mutants indicated that the accumulation and, by inference, replication of PLRV in the inoculated tissue were not affected by large deletions that abolish translation of RTP (Fig. 2B). Similar levels of RTP were

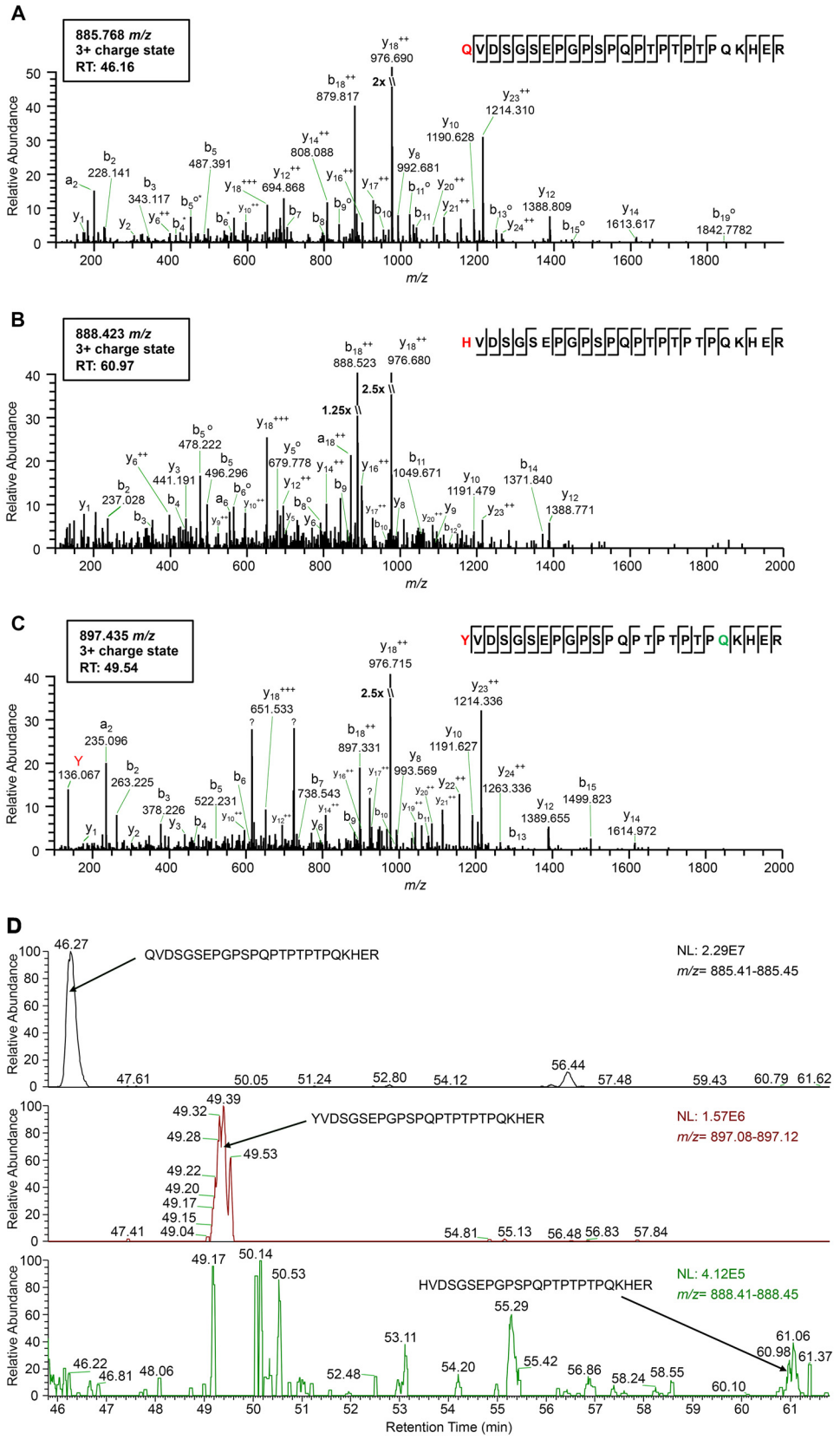

FIG 1 High-resolution mass spectrometry identifies the amino acid residue incorporated at the CP amber stop codon position during readthrough. (A to C) Tandem mass spectra (MS^2) of tryptic peptides spanning residues 209 to 233 in the PLRV RTP identified by affinity purification-MS analysis: K.Q_{209}VDSGSEPGPSPQPTPTPTPQKHER.F (*m/z*

(Continued on next page)

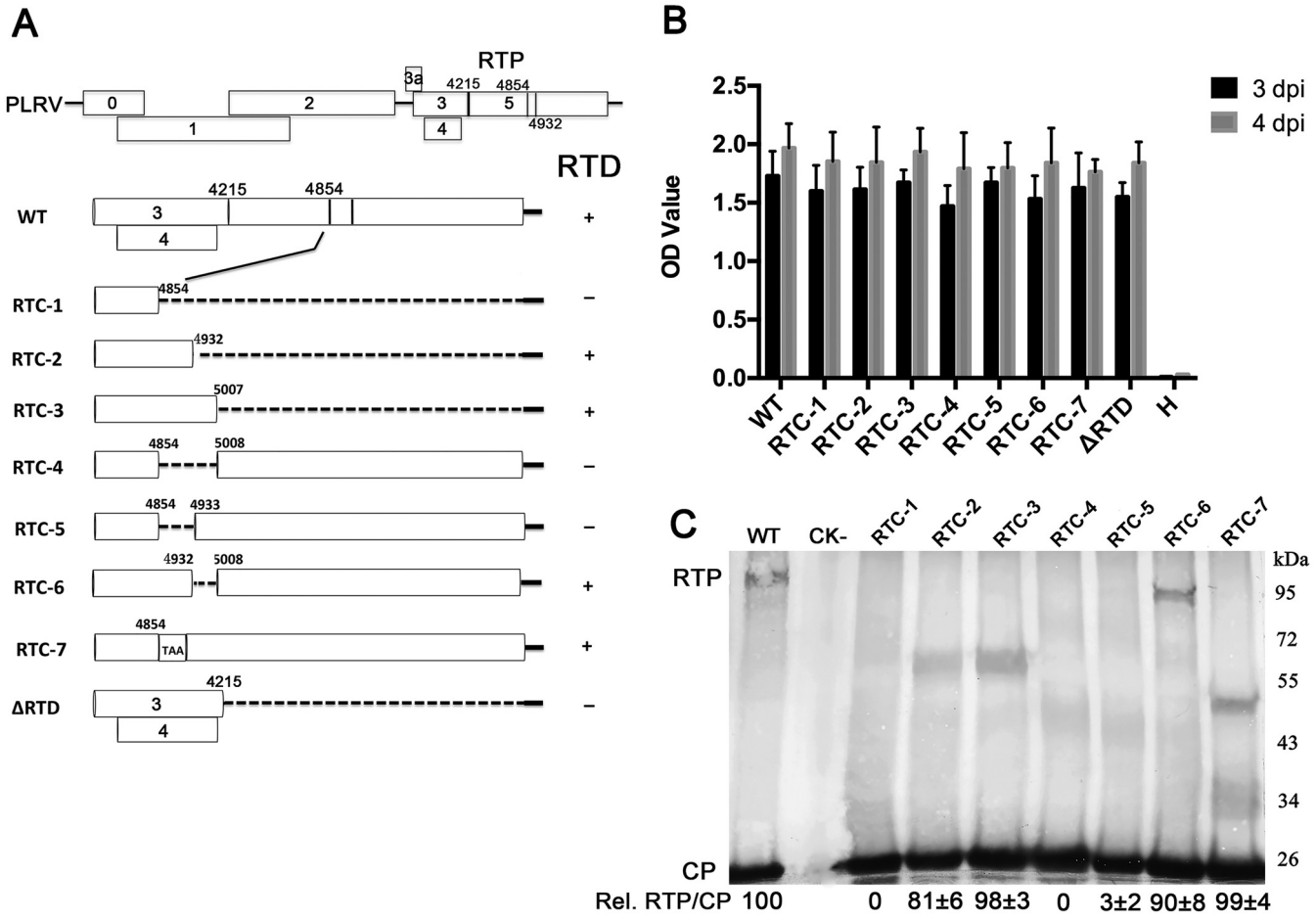

FIG 2 Identification of the PLRV DRTE responsible for RTP translation. (A) Schematic representation of the wild-type PLRV subgenomic RNA1 ORFs and the deletion or insertion mutations that were used to define the DRTE regulating readthrough. Detection of RTP translation based on the Western blots represented in panel C is indicated to the right of the schematic. (B) Accumulation of PLRV antigen, measured by DAS-ELISA, in *N. benthamiana* leaves 3 and 4 days after agroinfiltration with wild-type virus (WT) or the RTD deletion mutants. Healthy controls were agroinfiltrated with bacteria that do not contain the PLRV genome insert. H, noninfiltrated plant leaves. (C) Western blot analysis of PLRV proteins in *N. benthamiana* tissue 3 to 5 days following agroinoculation with wild-type PLRV or the RTP mutants. Relative readthrough (Rel. RTP/CP) was calculated as the RTP/CP ratio, with that for wild-type PLRV set as 100%. Values represent the means (± standard error) determined from three independent experiments.

detected by Western blotting using antibody recognizing the N terminus of the CP (34) in leaves infected with wild-type virus and the RTC-2, RTC-3, and RTC-6 mutants but not in those infected with mutant RTC-1, RTC-4, or RTC-5 (Fig. 2C). These results reveal that a sequence within nucleotides 4855 to 4932 is important and defines a specific distal readthrough element (DRTE) required for translation of RTP. Insertion of a stop codon,

FIG 1 Legend (Continued)

885.768) (A), K.H$_{209}$VDSGSEPGPSPQPTPTPTPQKHER.F (*m/z* 888.423) (B), and K.Y$_{209}$VDSGSEPGPSPQPTPTPTPQKHER.F (*m/z* 897.435) (C). Sequences show fragmentation along the peptide backbone and indicate the identity of residue 209 (red) and other ions that were used in peptide identification. For simplicity, only a representative amount of fragment ions in spectra are labeled. The ion peak highlighted in red indicates an immonium ion corresponding to the identity of a tyrosine residue at position 209. The residue highlighted in green indicates deamidation. RT, peptide retention time; ++, doubly charged ion; o, loss of H_2O; *, loss of NH_3; ?, contaminating fragment ions most likely from a coeluting peptide. (D) Relative abundances of the K.X$_{209}$VDSGSEPGPSPQPTPTPTPQKHER.F peptide isoforms identified in the same PLRV affinity purification from locally infected *N. benthamiana*. Extracted MS1 chromatograms for precursor ions with *m/z* values of 885.41 to 885.45 (top), 897.08 to 897.12 (middle), and 888.41 to 888.45 (low) detected between 45.80 and 61.80 min (retention time) are shown. Arrows indicate the MS1 peak corresponding to peptide K.Q$_{209}$VDSGSEPGPSPQPTPTPTPQKHER.F (retention time, 46.27 min) (A), K.Y$_{209}$VDSGSEP GPSPQPTPTPTPQKHER.F (retention time, 49.39 min) (B), and K.H$_{209}$VDSGSEPGPSPQPTPTPTPQKHER.F (retention time, 60.96 min) (C). The area under each peak is equal to the relative abundance of each peptide ion, with 100 on the *y* axis equaling the normalization (NL) value given in each panel.

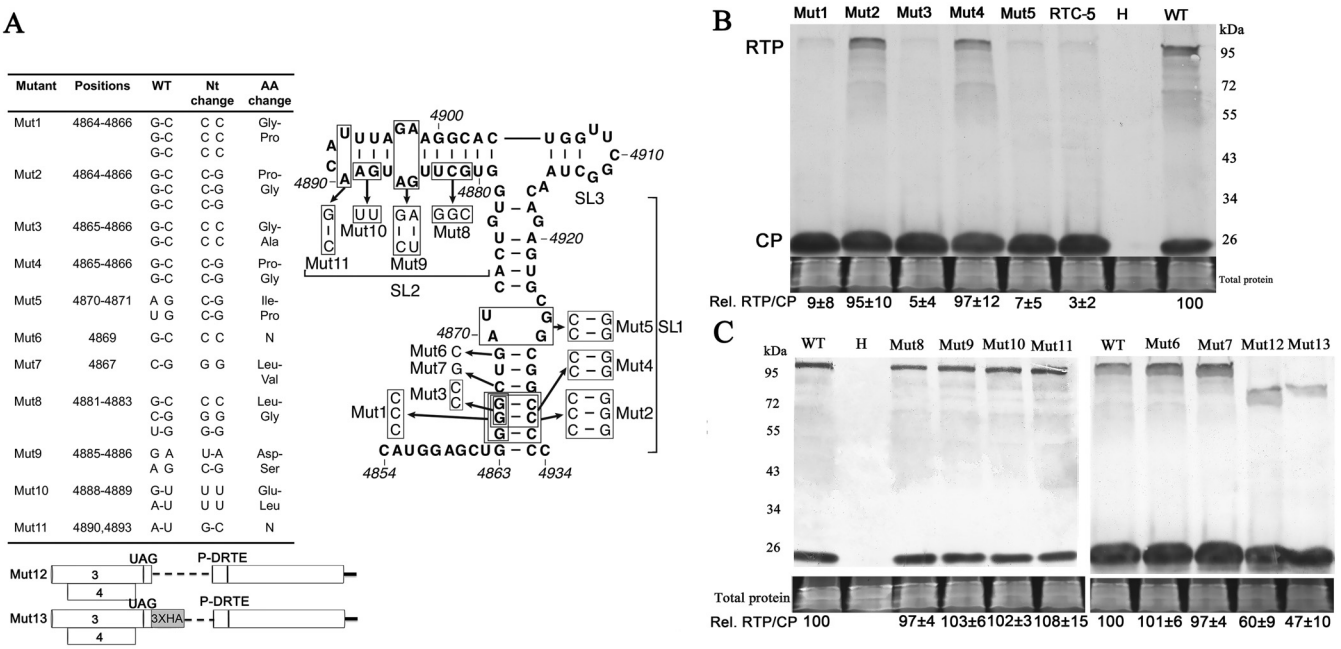

FIG 3 Stem-loop RNA structure of the distal element is required for RTP translation. (A) Predicted RNA secondary structure of the PLRV distal element and the mutants constructed for detecting RTP translation. (B) Western blot analysis of the role of stem-loop 1 in mediating RTP translation. (C) Western blot analysis of role of stem loops 3 and 4 in mediating RTP translation and the functional effects of the size and position of stem loop 1. Relative readthrough (Rel. RTP/CP) was calculated as the RTP/CP ratio, with that for wild-type PLRV set as 100%. Values represent the means (± standard error) determined from three independent experiments.

UAA, between nucleotides 4854 and 4855 (RTC-7), leaving the remainder of the open reading frame unchanged, did not abolish RTP accumulation (Fig. 2C), indicating that nucleotides 4855 to 4932 and not their encoded amino acids are needed for RTP translation.

To observe directly the synthesis of the RTP, we attempted *in vitro* translation of an *in vitro* transcript representing PLRV subgenomic RNA 1 (sgRNA1), which serves as the mRNA for ORF3a, -3, -4, and -5 in infected cells. However, we detected no RTP among translation products of PLRV sgRNA1 in wheat germ extract under conditions in which we were able to detect the CP and RTP of BYDV (data not shown). This reflects the results of Juszczuk et al., who were also unable to detect translation of the PLRV RTP in wheat germ extract (35).

A stem-loop RNA structure in the DRTE is required for RTP translation. Because RNA function is often controlled by its secondary structure, we investigated whether the potential secondary structure of the DRTE (nucleotides 4855 to 4932) plays a role in readthrough. The most stable predicted secondary structure of the PLRV DRTE forms the bulged, stem-loop structure shown in Fig. 3A (SL1 to SL3). To determine the existence and function, if any, of the helices and bulges in the predicted structure, mutations were introduced that would be expected to disrupt and, in some cases, restore predicted helices (Fig. 3A). Infectious clones of the PLRV genome containing these mutations in the DRTE were agroinfiltrated into *N. benthamiana* leaves, and tissue collected at 3 days postinoculation (dpi) was analyzed by Western blotting as a measure of RTP translation relative to wild-type (WT) virus (Fig. 3B). Changes of nucleotides 4864 to 4866 from GGG to CCC (Mut1) or of nucleotides 4865 and 4866 from GG to CC (Mut3), which were predicted to disrupt base pairing in stem 1 (Fig. 3A), reduced RTP to undetectable levels (Fig. 3B). Compensating changes to the opposite side of the stem that should restore base pairing and switch the wild-type GC base pairs to CG pairs (Mut2 and Mut4) (Fig. 3A) restored accumulation of RTP (Fig. 3B). Furthermore, alteration of unpaired nucleotides 4870 and 4871 from AU to CC in loop 1 (Mut5) (Fig. 3B), which would reduce the bulge in loop 1 to one base (C4924) and lengthen stem 1,

reduced RTP translation, whereas a G-to-C substitution at nucleotide 4869 (Mut6) (Fig. 3A), which would effectively enlarge the bulge, had no effect on RTP translation (Fig. 3C). A change from C to G at nucleotide 4867 that would cause a one-base-pair mismatch near the middle of stem 1 also had no noticeable effect on RTP translation (Mut7) (Fig. 3C). Mutations that would destabilize base pairing in stem 2, Mut8 and Mut10 (Fig. 3A), had no noticeable effect on RTP translation (Fig. 3C). Similarly, substitutions that would close the bulge in stem 2 (Mut9) or possibly convert the terminal loop to two bases (Mut11) (Fig. 3A) also had no effect on RTP translation (Fig. 3C). From this collection of mutants, we conclude that base pairing at the base of stem 1, but not its sequence, is necessary for efficient readthrough and that the predicted SL2 is unnecessary or may not exist. Thus, a stem-loop in the DRTE is necessary for readthrough, but its secondary structure outside the GC-rich basal helix is unknown (see structure probing data below).

In wild-type PLRV, the distance between the UAG codon and the start of the DRTE is 640 bases. Deleting nucleotides (nt) 4290 to 4840 decreased this distance from 640 to 90 nt, and RTP translation was reduced to 60% of the level found in wild-type virus (Fig. 3C, Mut12). Replacing nucleotides 4290 to 4840 with three copies of the human influenza virus hemagglutinin tag (90 nt total) reduced the relative level of RTP to 47% of that detected in wild-type virus (Fig. 3C, Mut13). This indicates that the distance and sequence between the stop codon and the DRTE are not critical for readthrough translation but can affect translation efficiency or readthrough protein stability.

Effect of mutations in the stem-loop sequence on systemic infection of plants. The luteovirid RTP functions in virus systemic infection, tissue tropism, and symptom development (17, 20, 26, 27); therefore, we tested the effects of several of the DRTE stem-loop mutations on disease symptoms and virus accumulation in whole plants. Mutants 1 to 7 (Fig. 3) were agroinoculated into hairy nightshade (HNS) (*Solanum sarrachoides*) plants at the 5- to 7-leaf stage, and plants were grown in the greenhouse for 9 weeks. Symptoms were observed several times a week, and virus accumulation in systemically infected leaves was monitored weekly using DAS-ELISA. Typical interveinal chlorosis symptoms were observed in all plants infected with wild-type PLRV, Mut2, Mut4, Mut6, and Mut7 beginning at 3 weeks postinoculation (wpi), and virus accumulated to similar levels throughout the experiments (Fig. 4). Mut3 and Mut5, which were impaired in RTP translation (Fig. 3), systemically infected all inoculated plants, but symptoms were not evident until 6 to 7 wpi. Mut1, which also was impaired in RTP translation, systemically infected 7 of 10 plants, but symptoms were not observed until 8 wpi. Virus accumulation in plants infected with Mut1, Mut3, and Mut5 increased slightly during the first 2 to 3 weeks and then decreased to background levels until 7 wpi, when the titer increased for the remainder of the experiment (Fig. 4). Plants inoculated with a mutant containing a deletion of the entire RTD, PLRV-ΔRTD, never developed symptoms; virus accumulated slightly during the first 3 wpi but then fell to background levels for the remainder of the experiment (Fig. 4).

Second-site mutations to recover a functional stem-loop structure. To determine if the emergence of wild-type-like symptoms and virus accumulation after 7 wpi in plants infected with Mut1, Mut3, and Mut5 was related to sequence changes, ORF3 to -5 sequences were amplified from systemically infected plant tissue collected at 9 wpi, cloned, and sequenced. No sequence changes were detected in products amplified from plants infected with wild-type PLRV or with Mut2, Mut4, Mut6, and Mut7. However, products from symptomatic plants systemically infected with Mut1, Mut3, and Mut5 all contained sequence modifications. Four of five clones sequenced from Mut1-infected plants contained a change in nucleotides 4864 to 4865 from CC to UG (Trp). The fifth clone contained a change in nucleotide 4864 from C to U. All five clones sequenced from Mut3-infected plants contained a C-to-G substitution at nucleotide 4865 (Gly), and all eight clones sequenced from Mut5-infected plants contained a C-to-U substitution at nucleotide 4871 (Leu). No additional sequence modifications were detected elsewhere in the ORF3/5 sequence.

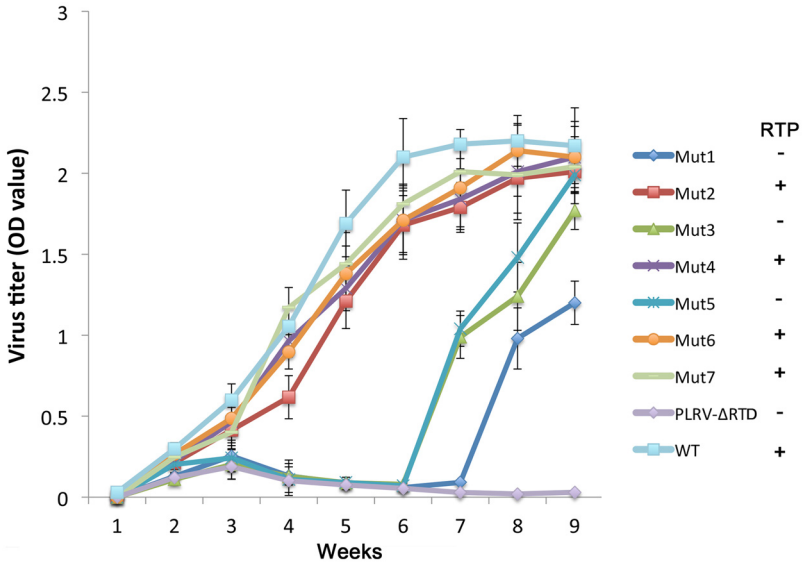

FIG 4 Time course of PLRV antigen accumulation in hairy nightshade plants systemically infected with wild-type PLRV and the various stem-loop mutants. Antigen was measured by DAS-ELISA in three randomly selected developing leaves from each of 40 plants. Data are displayed as average absorbance values (A_{405} minus A_{490}). Detection of RTP translation based on the Western blot data (Fig. 2) is indicated to the right of the graph. Only plants with an absorbance value above background at 3 weeks after agroinoculation were considered to be successfully agroinfected and were included in the calculations.

To determine if these second-site mutations restore wild-type levels of RTP accumulation, the nucleotide substitutions were introduced into the mutant clones, which were then agroinfiltrated into *N. benthamiana* leaves. Inoculated tissue was subsequently used to detect RTP by Western blotting. Indeed, these second-site changes in Mut1, Mut3, and Mut5, named Mut1R, Mut3R, and Mut5R, were all found to restore some level of translation of RTP (Fig. 5).

The above-described second-site mutations were predicted to restore stem-loop structures that more closely resemble those of wild-type virus. To test this experimentally, we performed selective 2′-hydroxyl acylation and primer extension (SHAPE) probing on RNA sequences that comprised these proposed structures and used these data to constrain MFOLD prediction of RNA structures. The wild-type structure resembled that predicted in Fig. 3A, with the exceptions that the three predicted, rather weak, base pairs at the distal end of SL2 did not form and that the predicted SL3 is also very weak if it exists at all, as some bases were highly SHAPE modified. Thus, the terminal SL2 loop consists of 14 bases, and SL3 is drawn with two base pairs but may simply be a large bulge (Fig. 5).

Surprisingly, the mutations in Mut1 and Mut3, which were predicted to disrupt the strong, GC-rich basal helix of SL1, had little effect on this helix, because the two strands of the helix simply slid in a 5′ or 3′ direction relative to each other to maintain substantial base pairing in most cases. For example, in Mut1, two of three bases in the CCC substitution base paired to two Gs in the central bulge of the wild-type SL1 (Fig. 5). The functional revertant, Mut1R, actually has a shorter basal helix than the wild type or Mut1. Mut5 folds as expected, with the extended basal helix, although the revertant Mut5R has only a (theoretically, but not apparent by SHAPE probing) slightly weaker helix with a CG-to-UG substitution.

A key, unpredicted structural feature common to the wild-type DRTE structure and the three functional revertants is that the bases in and around "SL3" are more highly modified (Fig. 5, red bases) than in the three nonfunctional mutants (no red bases). Thus, although drawn with two base pairs (by SHAPE-constrained MFOLD), SL3 appears to be a large loop in functional structures, whereas the stem of SL3 may form stably (with three base pairs, UGG · CUA, as in Fig. 3A) in the nonfunctional mutants. How base

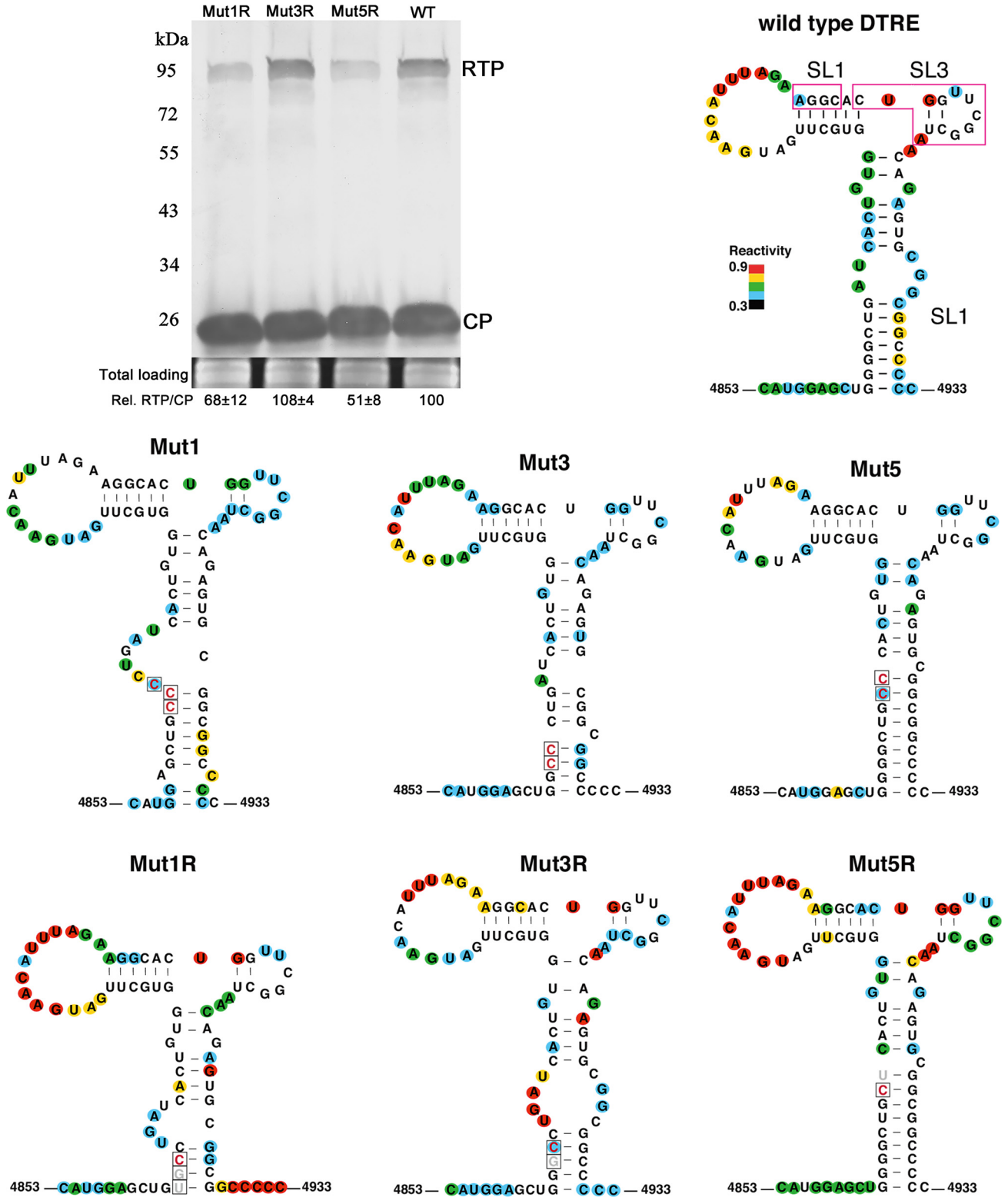

FIG 5 Secondary structures of the distal translation elements from wild-type virus (WT) and from stem-loop mutants Mut1, Mut3, and Mut5. The blot shows RTP translation by Mut1R, Mut3R, and Mut5R in agroinfiltrated *N. benthamiana* tissues at 3 dpi. Relative readthrough (Rel. RTP/CP) was calculated as the RTP/CP ratio, with that for wild-type PLRV set as 100%. Values represent the means (± standard error) determined from three independent experiments. Secondary structures of wild-type, mutant, and second-site mutant ("revertant") DRTEs that were recovered from plants that were symptomatic at 7 to 8 wpi are also shown. Each RNA was subjected to SHAPE probing, from which structure was predicted using SAFA and MFOLD software (see Materials and Methods). The degree of chemical modification ("single-strandedness") of each base is indicated by color-coded circles, with red indicating the most modified and blue the least. Uncolored bases showed no modification. Mutations are boxed, with constructed mutations in red and revertants in gray. Magenta boxes on wild-type RNA indicate bases predicted to base pair to the C-rich region adjacent to the leaky stop codon (Fig. 7).

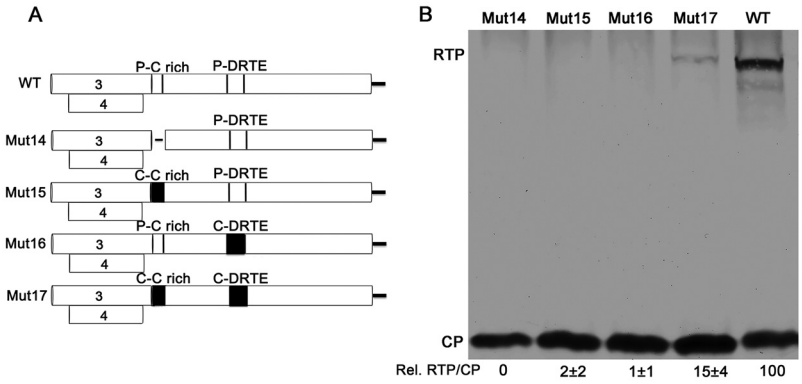

FIG 6 Communication between the DRTE and the C-rich domain is virus specific and indispensable for RTP translation. (A) Schematic of the chimeric ORF5 constructs, including a deletion of the PLRV C-rich domain (Mut14), a substitution with the homologous domain from CYDV-RPV (Mut15), a substitution of the PLRV DRTE with the homologous domain from CYDV-RPV (Mut16), and substitution of both PLRV domains with the homologous domains from CYDV-RPV (Mut17). (B) Western blot analysis of proteins in agroinfiltrated *N. benthamiana* tissue. Relative readthrough (Rel. RTP/CP) was calculated as the RTP/CP ratio, with that for wild-type PLRV set as 100%. Values represent the means (± standard error) determined from three independent experiments.

changes in the basal helix bring this about is not clear, but functionally this may be important, because, as presented below, base pairing between the DRTE and the C-rich domain adjacent to the leaky stop codon appears to be required for readthrough. The bases surrounded by the magenta boxes in the wild-type DTRE (Fig. 5), including all of SL3, are predicted to base pair to the upstream C-rich domain. If SL3 forms stably, as in the nonfunctional mutants, its sequence would be less available for base pairing to the C-rich motif 640 nt upstream.

Communication between the DRTE and the C-rich domain is virus specific and indispensable for RTP translation. To study the communication between, and the virus-specificity of, the C-rich domain and the DRTE, chimeric infectious clones were constructed that replaced the PLRV domains with *Cereal yellow dwarf virus* RPV (CYDV-RPV) (accession no. NC_004751; *Polerovirus*, *Luteoviridae*) domains based on their nucleotide alignment (Fig. 6A). The RTP was not detected when the C-rich domain of PLRV (nt 4222 to 4296) was deleted (Fig. 6, Mut14) confirming the finding by Brown et al. that the C-rich domain is essential for RTP translation (11). When the PLRV C-rich domain (nt 4222 to 4296) was replaced with the CYDV-RPV C-rich domain (nt 4366 to 4464) or when the PLRV DRTE (nt 4840 to 4935) was replaced with the CYDV-RPV DRTE (nt 5008 to 5103), no RTP translation was detected (Fig. 6B, Mut15 and Mut16, respectively). However, RTP translation was restored, albeit to a reduced level (15%) relative to that in wild-type PLRV, when both PLRV domains were replaced with the CYDV-RPV sequences (Fig. 6B, Mut17), indicating that these two domains are virus specific and communicate with each other.

Long-range base pairing between the 5′ end of the C-rich domain and the DRTE. Having established that communication between the C-rich domain and the DRTE is indispensable for RTP translation, we searched for potential long-distance base pairing between the stop codon-proximal C-rich domain and the DRTE. To exploit the power of phylogenetic variation, we aligned these regions of genomes of 47 luteovirids. This alignment revealed conserved codons in the DRTE that code for the amino acid motif [D/E]XG(X)$_6$DE near the center of the RTP (X = any amino acid), which is present in all but four viruses. Two of the exceptions differ at one codon from this consensus, and the others differ at two codons (including R replacing the 3′-terminal E codon). The penultimate D (aspartate) codon is always conserved. In PLRV, the EXG(X)$_6$DE-coding region spans bases 4858 to 4890 in the 5′ end of the DRTE (nt 4855 to 4932).

Using these alignments, we discovered that in all 47 luteovirid genomes examined, a 39-nt (usually ≤34-nt) tract in the DRTE, beginning with the 3′-terminal two codons

(GAY and GAR) of the [D/E]XG(X)$_6$DE motif, contains sequence with substantial complementarity to the 5′ end of the C-rich domain within 27 nt (9 codons) of the leaky stop codon (Fig. 7A). Most poleroviruses have a block of complementarity to the DRTE spanning 8 to 17 nt downstream of the stop codon. With three exceptions, there are at least six consecutive complementary bases between the 5′ end of the C-rich domain and the central domain of the DRTE. The exceptions had a minimum of nine base pairs with internal mismatches. PLRV has 16 MFOLD-predicted base pairs between the DRTE and the 27 nt adjacent to the leaky stop codon: 4217-UAGacuCCGGAUCAGaGCCU-4236· 4915-AGGCaCUGGUUCGGCUA-4899 (mismatches are in lowercase). In most of the 47 luteovirids, additional base pairing between the C-rich domain and the DRTE was predicted, but the positions of these additional complementary tracts are not as highly conserved as those in Fig. 7A. Importantly, MFOLD predicts no more than five consecutive potential base pairs between the CYDV-RPV DRTE and the PLRV C-rich domain and vice versa, which may explain why these combinations of different viral elements yielded no readthrough (Fig. 6). In summary, given the substantial tracts of complementarity in these highly localized regions of all the 47 luteovirid genomes, despite substantial sequence variation, it is highly likely that these sequences do indeed base pair to facilitate readthrough.

To determine experimentally whether these putative long-distance base-pairing interactions in the readthrough process can be detected functionally, five mutants were designed to disrupt the base pairing between the C-rich domain and the DRTE. Two 15-nt deletion mutants, Δ4222–4236 and Δ4897–4911, and a 12-nt deletion mutant, Δ4222–4233, removed a majority of the complementary bases without changing reading frame. The fourth mutant (Mut4222–4236-AA) contained point mutations that changed nine of the 15 complementary nucleotides in the DRTE sequence to disrupt base pairing without altering the amino acid sequence (Fig. 7B). The fifth mutant (Mut4233–4236-AGGA), modified the nucleotides at positions 4233 to 4236 from GCCU to AGGA (Fig. 7B). RTP was not detected in Western blots when either 15-nucleotide sequence was deleted (Fig. 7B), and RTP accumulated to only ~10% of wild-type levels in the other three mutants, which would impair but not eliminate base pairing between the two domains (Fig. 7B). These results are consistent with a requirement for long-range base-pairing interaction between the C-rich domain and the DRTE for efficient readthrough. To check whether compensatory mutations could restore readthrough translation, two additional mutants (Mut4222–4236-AA-C and Mut4233–4236-AGGA-C) were constructed. These would be predicted to restore base pairing between the C-rich domain and the DRTE (Fig. 7B), but neither of the mutants restored an accumulation of RTP (Fig. 7C). This may be due to unintended local folding of the mutant RNA that hinders the long-distance interaction or to negative effects of the amino acid changes in the RTD on virus accumulation.

RTP mutants infect fewer phloem-associated cells in all tissue types. Accumulation of PLRV in agroinfiltrated leaves was not affected by any of the RTD mutants regardless of deletion size or the detection of translated RTP (Fig. 2B), consistent with previous reports that the RTD has no effect on virus replication (26). Furthermore, a loss of RTP did not prevent systemic movement of virus within the first 2 to 3 wpi, although virus accumulation in systemically infected tissue was reduced (Fig. 4). Tissue printing was used to compare the spatial distribution of infection foci in tissues systemically infected with wild-type virus, stem-loop mutants Mut1 and Mut7, and PLRV-ΔRTD. Fewer infection foci were observed in leaves and stems infected with Mut1 than in those infected with Mut7 at 3 wpi, and the infection foci were infrequent and isolated (Fig. 8A, left column, and B). The number and distribution of infection foci in tissue systemically infected with WT PLRV and PLRV-ΔRTD were similar to those in tissue infected with stem-loop mutants Mut7 and Mut1, respectively (Fig. 8A, right column, and B). Tissue examined at 9 wpi indicated similar patterns and intensities of infection foci for stem-loop mutants Mut1 and Mut7 (Fig. 8C and D), as well as WT PLRV, whereas in tissue infected with PLRV-ΔRTD, only a few widely scattered infection foci were

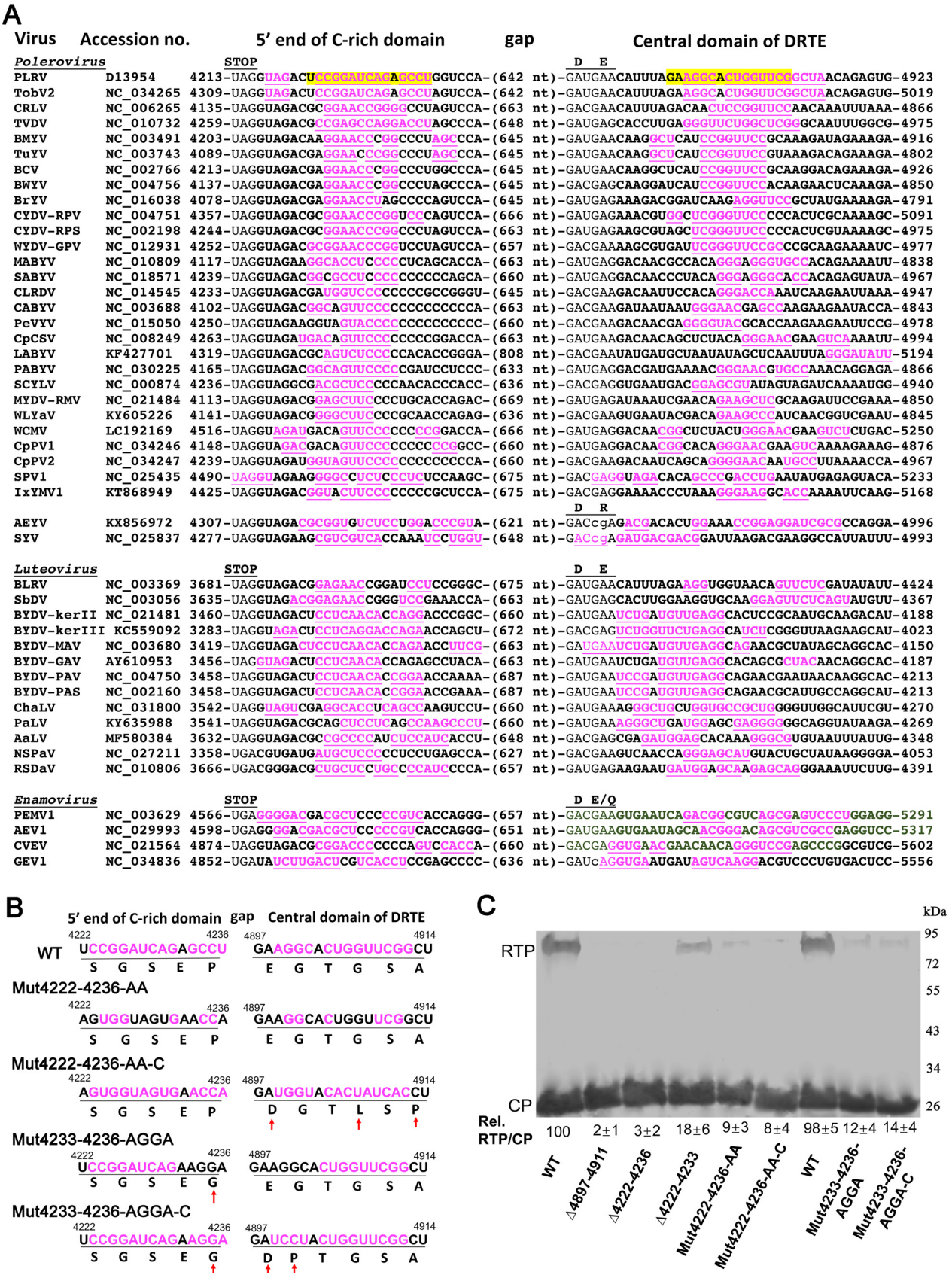

FIG 7 Long-range base pairing between the DRTE and 5′ end of C-rich domain. (A) Alignment of potentially complementary regions of the C-rich motif adjacent to the leaky stop codon (lightface) and the portion of the DRTE adjacent to the conserved EXG[X]$_6$DE motif. The bases coding for DE (GAYGAR)

(Continued on next page)

observed (Fig. 8C and D). The intensity of the staining of individual infection foci was comparable for all virus constructs, suggesting that RTP does not affect virus replication/accumulation in individual cells but does affect the establishment of new infection foci.

DISCUSSION

Termination codon readthrough is recognized as a mechanism of expression for a growing number of viral and cellular proteins (2, 36). Readthrough signals have been classified into three main groups based on either a sole requirement for local sequence context types I, or the additional involvement of a 3′ structural element (types II and III) (1, 9). In type I, tobamovirus-like, the six bases at the 3′ end of the stop codon usually conform to the motif UAG-CAA-UYA, and in type II, the stimulatory context is generally UGA-CGG or UGA-CUA and a 3′ RNA structure (10). Type III signals are exemplified by that of the retrovirus *Moloney murine leukemia virus* (MuLV), which possesses a 3′ stimulatory RNA structure in the form of an RNA pseudoknot located eight nucleotides downstream from the *gag* UAG codon (37). In recent years, several groups have proposed that the stop codon readthrough mechanism is specifically regulated by *cis*-acting RNA elements downstream of the first stop codon that may exist to generate proteome diversity in response to changing environmental conditions, and the importance of pseudoknots and other secondary structures in mediating biological functions has been documented in an increasing number of systems (37–41).

This work provides *in planta* confirmation of previous studies on BYDV-PAV, which found similar local and distant sequences to be required for ORF3 (CP) stop codon readthrough (11). In that case, the evidence was based on direct *in vitro* translation and reporter assays in protoplasts. Here, we show that similar sequences apply to readthrough control in the context of replicating virus as it moves through the whole plant. The surprising difference is that we were unable to detect RTP translation in wheat germ extract. To our knowledge, no lab has observed readthrough of the PLRV ORF3 stop codon *in vitro* with a natural tRNA population. Tacke et al. (31) first reported PLRV ORF3 stop codon readthrough via infection and reporter gene expression in protoplasts only. Juszczuk et al. reported detection of the RTP upon translation of PLRV sgRNA1 in wheat germ extract only in the artificial situation of adding tRNAs from a yeast strain that expresses suppressor tRNAs (35). Although we did not detect *in vivo* translational readthrough directly, it is very difficult to explain our results by any other event. Perhaps the translation conditions for PLRV *in vivo* may be different from those *in vitro*, or alternatively, wheat germ extract lacks tRNAs present in the dicot hosts of PLRV. The mutations that prevent RTP accumulation do not affect virus replication or stability or the overall translation efficiency of sgRNA1, as indicated by constant levels of CP in plants expressing or not expressing RTP (Fig. 2 and 3). Given the similar sequence requirements found for PLRV RTP accumulation in plants and for directly detected

FIG 7 Legend (Continued)
are in lightface, with exceptions in lowercase. Complementary bases are in underlined magenta, base positions are indicated at ends, and the gap length between the two regions is in parentheses. Regions in the PLRV sequence highlighted in yellow indicate the bases deleted in the Δ4222-4236 and Δ4897-4911 mutants. Abbreviations not defined elsewhere: TobV2, *Tobacco virus 2*; CRLV, *Carrot red leaf virus*; TVDV, *Tobacco vein distortion virus*; BMYV, *Beet mild yellowing virus*; TuYV, *Turnip yellows virus*; BCV, *Beet chlorosis virus*; BrYV, *Brassica yellows virus*; WYDV, *Wheat yellow dwarf virus*; MABYV, *Melon aphid-borne yellows virus*; CLRDV, *Cotton leafroll dwarf virus*; CABYV, *Cucurbit aphid-borne yellows virus*; PeVYV, *Pepper vein yellows virus*; CpCSV, *Chickpea chlorotic stunt virus*; LABYV, *Luffa aphid-borne yellows virus*; PABYV, *Pepo aphid-borne yellows virus*; SCYLV, *Sugarcane yellow leaf virus*; MYDV-RMV, *Maize yellow dwarf virus-RMV*; WLYaV, *Wheat leaf yellowing-associated virus*; WCMV, *White clover mottle virus*; CpPV, *Chickpea polerovirus*; SPV1, *Strawberry polerovirus 1*; IxYMV1, *Ixeridium yellow mottle virus 1*; AEYV, *African eggplant yellows virus*; SYV, *Sauropus yellowing virus*; BLRV, *Bean leafroll virus*; SbDV, *Soybean dwarf virus*; ChaLV, *Cherry-associated luteovirus*; PaLV, *Peach-associated luteovirus*; AaLV, *Apple-associated luteovirus*; NSPaV, *Nectarine stem-pitting-associated virus*; RSDaV, *Rose spring dwarf-associated virus*; PEMV1, *Pea enation mosaic virus 1*; AEV1, *Alfalfa enamovirus 1*; CVEV, *Citrus vein enation virus 1*; GEV1, *Grapevine enamovirus 1*. (B) Diagram of the wild-type PLRV and mutants used for testing the effect of the complementary long-range base-pairing. Mut4222–4236-AA, replacement of nine out of 15 nucleotides in the 4222–4236 domain and no changes of original amino acids. Mut4222–4236-AA-C, complementary mutant of Mut4222–4236-AA in the DRTE; Mut4233–4236-AGGA: replacement of GCCU by AGGA in the domain of 4233–4236. Mut4233–4236-AGGA-C, complementary mutant of Mut4233–4236-AGGA. Arrows indicated the amino acid changes. (C) Western blot analysis of proteins in agroinfiltrated *N. benthamiana* tissue. Δ4222–4236, deletion of nt 4222 to 4236 in PLRV C-rich domain; Δ4897–4911, deletion of nt 4897 to 4911 in the DRTE; Δ4222–4233, deletion of nt 4222 to 4233. All the deletion mutations also did not change the ORF. Relative readthrough (Rel. RTP/CP) was calculated as the RTP/CP ratio, with that for WT PLRV set as 100%. Values represent the means (± standard error) determined from three independent experiments.

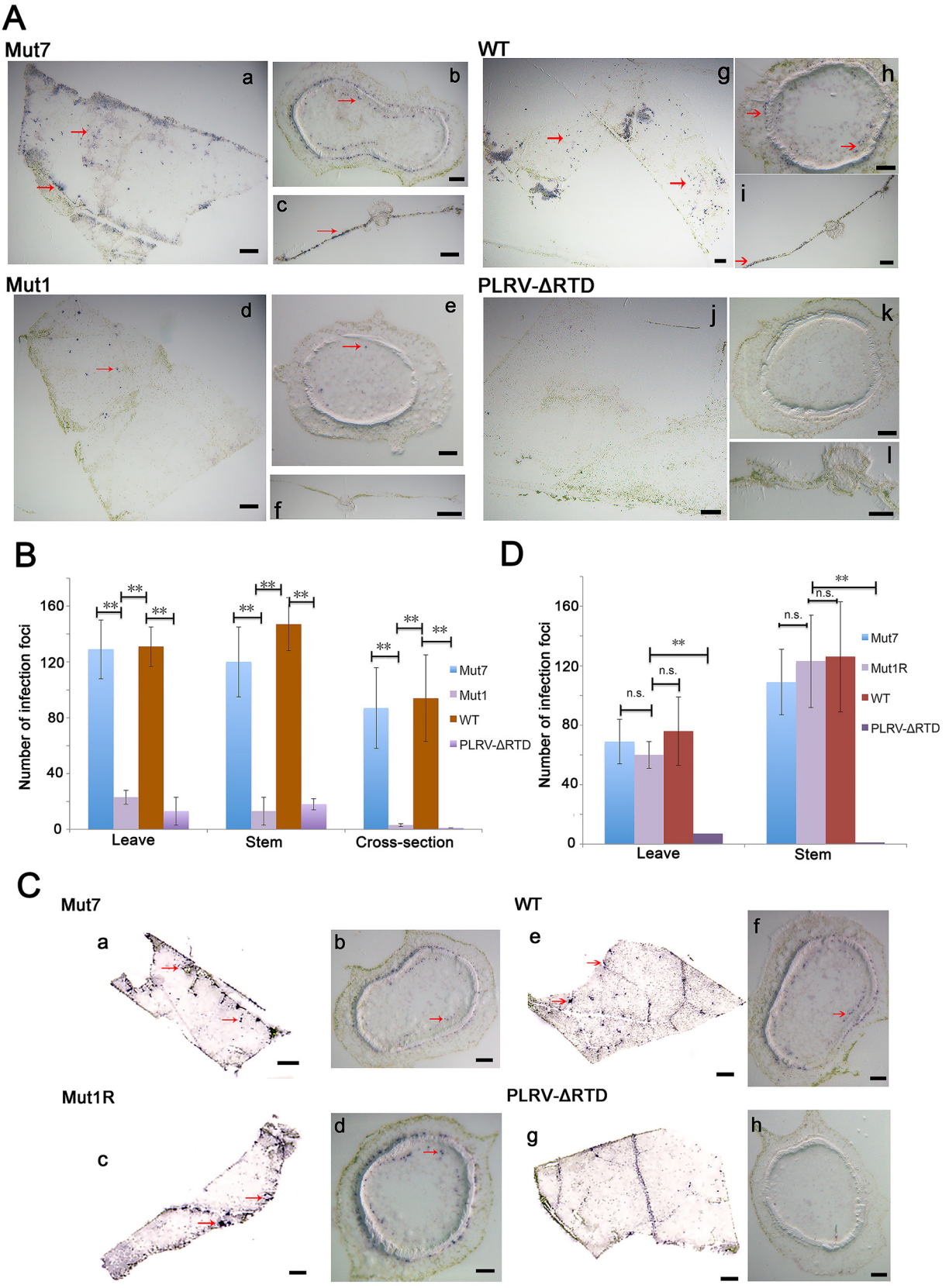

FIG 8 (A and C) Tissue prints showing PLRV infection foci in HNS stem and leaf tissues systemically infected with Mut1, PLRV-ΔRTD (which does not translate RTP), and Mut7 (which translates RTP at near-wild-type levels). Tissue was collected at 3 wpi (A) and 9 wpi (C). By 9 wpi Mut1 has accumulated compensatory mutations that restored RTP translation. (B and D) Actual counts of infection foci. Tissue prints were developed with

(Continued on next page)

readthrough in BYDV-PAV, we conclude that the mutations in the PLRV RTD are affecting control of stop codon readthrough.

Like BYDV-PAV, PLRV RNA contains two domains required for readthrough translation of the RTP: the CCN-NNN repeats beginning shortly downstream of the UAG and a distal sequence located 640 nt downstream within ORF5. The BYDV distal element maintained function when moved 2 kb from the stop codon (11). We also detected RTP when the length between the C-rich domain and distal stem-loop was reduced, indicating that the position of the distal element is not critical for the readthrough process in luteovirids. Brown et al. (11) predicted base pairing between these domains for some BYDV isolates. Our findings of virus specificity of the C-rich domain and DRTE, the presence of significant complementary tracts in precisely the same regions of the genomes of the 47 luteovirids (Fig. 7), and the requirement for these complementary sequences for readthrough of the PLRV ORF3 stop codon strongly support the requirement for this base pairing.

Based on SHAPE probing, the RNA sequence in the DRTE proposed to base pair to the C-rich motif resides at the distal end of a branched stem-loop structure that protrudes from the genome via a GC-rich basal helix. This likely ensures the accessibility of the sequence (boxed in Fig. 5) for long-distance interactions, as has been observed for the long-distance base pairing required by other structures for both cap-independent translation initiation and ribosomal frameshifting in the genus *Luteovirus* and certain members of the *Tombusviridae* (4, 36, 42). A functionally similar, but structurally different, interaction between a DRTE and sequence adjacent to the leaky stop codon is required for readthrough in tombusviruses (13). In that case, the DRTE is located in the 3′ UTR, 3.5 kb downstream of the leaky stop codon, readthrough of which results in translation of the viral RNA-dependent RNA polymerase. The 6-nt DRTE base pairs to a bulge in a very large stem-loop structure (called the proximal readthrough element [PRTE]) immediately adjacent to the leaky stop codon. Betanecroviruses (*Tombusviridae*) contain an additional readthrough-enhancing stem-loop adjacent to the PRTE (43). Alternative base pairings adjacent to the DRTE appear to regulate the readthrough efficiency of tombusviruses (13). In its most active form, the tombusvirus DRTE is a loop on a short stem-loop. The luteovirid DRTEs differ in that the tracts of sequence complementary between DRTE and stop codon-proximal sequence (5′ end of C-rich domain) are predicted to be longer than those in tombusvirids, which are mostly 6 nt and not longer than 9 nt (13). For example, PLRV and BYDV-PAV RNAs are predicted to form 16 and 12, respectively, base pairs between the DRTE and the 5′ end of the C-rich domain (Fig. 7). Moreover, luteovirids lack the highly stable stop codon-proximal stem-loop present in tombusvirids, while tombusvirids lack the CCNNNN repeat motif.

While mutations predicted to disrupt the long-distance base pairing between the DRTE and the stop codon-proximal region indeed reduced virus (RTD) accumulation, compensating mutations predicted to restore the long-distance base pairing did not restore virus to levels higher than those obtained with the disruptive mutants (Fig. 7C). This may be due to any of the following: (i) the RNA structure was altered by the compensating mutations in such a way as to render the mutant bases unavailable for long-distance base pairing due to new local base pairing of these bases to adjacent sequence, (ii) the thermodynamic stability of the new base pairs may be too low (or high) to facilitate the appropriate level of readthrough, (iii) a specific sequence is required (but not conserved among luteovirids), or (iv) the amino acid changes necessary to make the compensating mutations impaired RTD function or stability,

FIG 8 Legend (Continued)
antibodies to PLRV, and virus was visualized as blue-stained foci of indoxyl precipitate. The prints were photographed under a microscope at a magnification of ×10 to ×35. Graphs show the average of 15 infection foci and represent the number of virus infection foci in the immunoprint cross sections photographed under a microscope. **, significant differences in the number of stained foci ($P < 0.01$ by one-way analysis of variance [ANOVA]); n.s., no significant difference. (A) Bars in panels a, c, d, f, g, i, j, and l represent 1 mm, and those in panels b, e, h, and k represent 100 μm. (C) Bars in panels a, c, e, and g represent 1 mm, and those in panels b, d, f, and h represent 100 μm.

reducing virus accumulation despite readthrough being restored. Thus, while restoring virus levels via compensating mutations would virtually prove that long-distance base pairing facilitates readthrough, the inability to restore virus levels by mutations designed to be compensating does not disprove that such base pairing is required for readthrough. Given the strong phylogenetic conservation of long-distance base pairing by sequences in the DRTE, it is highly likely that this base pairing occurs and facilitates readthrough.

Several of the PLRV DRTE bases predicted in the long-distance interaction are constrained in SL2 and possibly SL3 (magenta box in Fig. 5), which would make them inaccessible to the C-rich domain bases. However, parts of SL2 and SL3 in wild-type DRTE and the functional mutants show much more benzoyl cyanide (SHAPE) modification (single strandedness) than in the nonfunctional mutants (Fig. 5), so they may indeed be available for long-distance pairing. This leads us to propose that the single-stranded bases in SL3 (which may actually be a single-stranded bulge) initiate base pairing to the C-rich domain, causing SL2 to "unzip" as the SL2 bases then pair to the C-rich motif; i.e., the SL3 bases form the nucleation site for formation of the long-distance pairing to the C-rich domain which in its final 16 bp form may be more stable than SL2 and SL3 within the DRTE. Obviously, additional experiments are necessary to test this hypothesis.

The finding that Gln, Tyr, or His occupies the stop codon site of the CP ORF indicates that $tRNA^{Gln}$, $tRNA^{Tyr}$, and $tRNA^{His}$ can be incorporated at the PLRV CP UAG termination codon. This is the first report of the amino acids incorporated in the leaky stop codon of a luteovirid CP-RTP protein. $tRNA^{Gln}$ and $tRNA^{Tyr}$ have been identified as efficient suppressors of the UAG codon in other virus-host systems (1, 44). Thus, as in other viral systems (and unlike the selenocysteine system), the *cis*-acting sequences that promote readthrough appear to act more to keep release factor out of the ribosome, rather than to facilitate insertion of any particular aminoacyl tRNA. Further work is required to determine if $tRNA^{Gln}$-Gln is favored in the PLRV CP ORF stop codon because it may have a higher concentration in *N. benthamiana* than $tRNA^{Tyr}$ and $tRNA^{His}$ or because $tRNA^{Gln}$ simply has a higher affinity for UAG than the His and Tyr tRNAs.

This work is also significant because we are unaware of any previous reports that a $tRNA^{His}$ can be recognized at a UAG codon. Zhang et al., found high initial misreading *in vitro* of near-cognate codons by some tRNAs, such as $tRNA^{Glu}$ and $tRNA^{His}$ (45, 46). We suspect that $tRNA^{His}$ in the UAG stop codon may be caused by the unconventional base interactions, and we also cannot rule out the possibility that there might be a very low level of viral RNAs in the infecting quasispecies with mutations in the CP stop codon.

In principle, there are several ways that long-distance *cis*-acting RNA structures could affect stop codon readthrough: (i) interference with release factor entry into the A site and conformation through steric hindrance, sequestration, or modulation of other proteins involved in termination (47, 48); (ii) recruitment of other factors that modulate release factor function (49); or (iii) induction of ribosomal pausing over the stop codon, increasing the time for the action of a tRNA (50, 51). Precisely how the DRTE mediates readthrough remains unknown, but possibilities include interaction with the C-rich domain forming a higher-order RNA structure near the CP stop codon that promotes ribosome stalling and/or the recruitment of other factors that inhibit translation release or factor function or promote suppressor tRNA utilization.

Another question is the role of the CCNNNN repeat motif. The luteovirid DRTEs base pair to the first one or two units of this motif, which in the case of PLRV starts at the 7th codon (21st base) after the leaky UAG codon. However, Brown et al. (11) showed that a minimum of eight CCNNNN repeats were required for readthrough in BYDV RNA. No such repeats have been reported for readthrough in the *Tombusviridae* or any other viral or cellular leaky stop codon.

Host adaptation is the main selective pressure to control virus genetic diversity and restrict virus genome variability. CP readthrough and the extensive use of this mechanism for host adaptation in vector-borne plant viruses have been well studied (17, 22,

27, 52–54). The readthrough protein of PLRV plays key roles in several processes, including virus movement, accumulation, and symptom development in plant hosts, as well as in the virus life cycle within aphids. In this study, sequence reversion to maintain the stem-loop structure suggests that stem-loop-mediated RTP expression is very important for PLRV infection in hosts. Indeed, several investigators have found that luteovirus RTP restored translation by reversion or pseudoreversion in mutagenesis experiments (17, 22, 25). Our previous work found reversions of a frameshift mutation in the PLRV ORF5 that generated a truncated RTP. The revertants were able to translate a full-length RTP and restore wild-type movement and symptom development (25). Pseudorevertants of the beet western yellows virus (BWYV) RTP also restored the reading frame, contributing to the ability of the virus to move efficiently in phloem and to accumulate to wild-type levels in plants (17). Also, some point mutations of BWYV were reversed in the readthrough mutants that strongly inhibited virus accumulation *in planta* or transmission by aphids, indicating that a functional RTP is required for these processes (22). Consistent with studies on BWYV, in our study, we also found that PLRV RTD is not essential for efficient virus multiplication in the phloem cells but promotes virus movement to increase the rate at which new infection foci are established and expand (Fig. 8). All these findings suggest there may be some conserved RTP functions that all luteovirids have adopted to infect hosts.

In general, a higher titer of virions in the phloem can facilitate virus transmission by vectors from one plant to another (55, 56). In this study, we found that host selection pressure shapes RNA (DRTE) structure to maintain function beyond coding information. PLRV moves more efficiently to new infection foci when RTP is expressed. Increasing the number of infection foci and in turn virus titer will also facilitate increased efficiency of virus acquisition by aphid vectors and virus transmission to new hosts.

MATERIALS AND METHODS

Plasmid generation and inoculation. Recombinant cDNA of PLRV (accession number KP090166) mutants used in this study were generated using specifically designed primers according to the previously described yeast recombination method (33). All the primers are available upon request. Briefly, by using a set of restriction enzymes, BsrGI and XhoI or BsrGI and BsaI, the plasmid pBPY, a yeast-bacterial shuttle vector containing a full-length cDNA of PLRV, was linearized and dephosphorylated with alkaline phosphatase (New England BioLabs, Ipswich, MA, USA) to inhibit recircularization. The short insertion fragments containing the mutated region were PCR amplified from pBPY with primers homologous to their junctions. Yeast transformation was carried out based on the lithium acetate (LiAc)–single-stranded carrier DNA–polyethylene glycol (PEG) method (57). Total DNA, including the recombinant plasmid DNAs, was rescued from pooled yeast colonies grown on SD-Trp medium agar plates (Clontech, Mountain View, CA) and then used to transform *Escherichia coli* strain DH5α. Plasmid DNAs recovered from DH5α were sequenced to verify sequence integrity. *Agrobacterium tumefaciens* strain LBA4404 was transformed with plasmids extracted from DH5α and used for agroinfiltration of *N. benthamiana* and *S. sarrachoides* (HNS) as previously described (58).

Protein extraction and Western blot analysis of RTP translation. All *N. benthamiana* plants used in this study were grown in a greenhouse maintained at 25 $\pm$ 2°C with a 16:8-h photoperiod, and 4 to 6 leaves were used for infiltration. Agroinfiltrated *N. benthamiana* leaf tissues were ground to a powder in liquid nitrogen using a pestle and mortar; 100 mg was resuspended in 0.5 ml of cold extraction buffer containing 50 mM Tris-HCl (pH 6.8), 2.5% SDS, 10% glycerol, and 100 mM dithiothreitol (DTT) (added fresh) and incubated on ice for ~20 min with occasional vortexing. Samples were centrifuged at 16,000 $\times$ *g* for 5 min, and 50 μl of the supernatant was diluted 1:1 in 2$\times$ Laemmli sample buffer (Bio-Rad, Hercules, CA) supplemented with β-mercaptoethanol (5%, vol/vol) (BME). For Western blotting, samples were incubated at 100°C for 8 to 10 min, separated on a 10% Mini-Protean TGXTM precast gel (Bio-Rad), and transferred to nitrocellulose. SDS-PAGE, transfer, and Western blotting were performed as described previously (59). PLRV CP and RTP were detected using by using a monoclonal antibody, SCR3, that recognizes the N terminus of the CP (34) as the primary antibody. The blotted signal was visualized using chemiluminescence according to the manufacturer's manual (GE Healthcare, USA), and signal band quantification was measured with ImageJ software (https://imagej.nih.gov/ij/). All experiments were repeated at least three times.

***In vitro* translation assay.** DNA templates were amplified by PCR using Q5 high-fidelity DNA polymerase (New England BioLabs) with the primers TAATACGACTCACTATAGGGAGAGGACAAAAGAAC ACTGAAGGAGCTC (forward) and AGTACTACACAACCCTGTAAGAGGATCCTGGCT (reverse) (the T7 promoter is underlined). The RNAs were synthesized by *in vitro* transcription with T7 polymerase using the MEGAscript kit (Ambion). RNA was purified on spin columns according to the manufacturer's instructions (Zymo Research, Irvine, CA, USA), and RNA integrity was verified by 0.8% agarose gel electrophoresis. The RNA concentration was determined by spectrophotometry using a NanoDrop 2000 instrument (Thermo Scientific). *In vitro* translation reactions were performed in wheat germ extract (Promega, Madison, WI,

USA) as described previously (60). Nonsaturating amounts of RNAs (700 ng) were translated in wheat germ extract in a total volume of 20 μl with a [^{35}S]methionine-labeled amino acid mixture and 83 mM potassium acetate, based on the manufacturer's instructions. Translation reaction mixtures were incubated at room temperature (25°C) for 90 min. Translation products were separated on a NuPAGE 4 to 12% Bis-Tris gel (Invitrogen), detected with a Pharox FX Plus Molecular Imager, and quantified with Quantity One one-dimensional analysis software (Bio-Rad).

RNA sequence and secondary structure analysis. Nucleotide sequences from different polerovirus genes (ORF3/5) encoding RTP were aligned using **mu**ltiple **s**equence **c**omparison by **l**og **e**xpectation (MUSCLE) (http://www.ebi.ac.uk/Tools/msa/muscle/) (61). The aligned sequences were edited and converted into diagrams using GeneDoc (http://iubio.bio.indiana.edu/soft/molbio/ibmpc/genedoc-readme.html). For alignment of 47 luteovirid RTD-related nucleotide sequences, an online version of CLUSTALW 2.1 software was used with the default "slow/accurate" parameters (http://www.genome.jp/tools/clustalw/), and the amino acids encoded in the DRTE region were also listed. RNA secondary structures in the distal element of wild-type PLRV and the mutants were predicted using the RNAfold web server (http://rna.tbi.univie.ac.at/cgi-bin/RNAWebSuite/RNAfold.cgi) based on thermodynamic prediction of minimal free energy (MFE) (62). Long-distance base pairing was found by fusing a sequence spanning the first 100 nt downstream of the leaky stop codon with the aligned (see above) DRTE sequence into a single file and performing MFOLD under default conditions (63).

Selective 2′-hydroxyl acylation and primer extension (SHAPE) probing was performed as described previously using benzoyl cyanide as the modifying reagent (64). The template was generated by *in vitro* transcription of a DNA sequence spanning bases 4841 to 4964 of PLRV fused to a downstream "SHAPE cassette" sequence to which the primer for reverse transcription was annealed. As described previously (65), 500 ng of $PLRV_{4841-4964}$ RNA generated by *in vitro* transcription was denatured and renatured in SHAPE buffer (50 mM HEPES-KOH [pH 7.2], 100 mM KCl, and 8 mM $MgCl_2$) by heating and slow cooling. RNA was modified by mixing a 1/10 (vol/vol) ratio of renatured RNA with 60 mM benzoyl cyanide (Sigma) in anhydrous dimethyl sulfoxide (DMSO) (Sigma). After 2 min, the RNA was mixed with 4-fold excess tRNA and precipitated with ethanol in 0.3 M sodium acetate. Control RNA was treated with the same amount of DMSO without benzoyl cyanide. The primer for primer extension (5′-TGATCTTTTTGGGCGAGACATCC-3′) was 5′ end labeled with [γ-^{32}P]ATP. Radioactive primer extension products were run in a 6 M urea–6% polyacrylamide gel and exposed to a phosphorimager screen. The reactivity of each nucleotide (color coded in Fig. 5) was quantified using SAFA software (66). These data were then used as constraints in MFOLD (63) to predict a structure consistent with SHAPE reactivities (63, 67).

Analysis of virus in infected tissue. Virus accumulation in agroinoculated plants (three plants for each sample) was detected by using DAS-ELISA as described previously by Lee et al. (68). Progeny viruses in systemically infected plants were analyzed by reverse transcription-PCR (RT-PCR) and sequencing of the RT-PCR products. Tissue immunoblot analysis was performed on plant tissues infected with the various mutants at 4 wpi essentially as described previously by Lee et al. (68). For stems, single cuts were made across the axis and the cut surface pressed directly onto nitrocellulose membranes that were treated with 0.2 M $CaCl_2$ prior to blotting. Tissue prints were allowed to air dry and stored at 4°C until the end of the experiment, at which time the samples were analyzed under the same conditions. PLRV coat protein was detected in tissue blots using anti-PLRV immunoglobulin and goat anti-rabbit immunoglobulin conjugated to alkaline phosphatase (1:5,000) as the secondary antibody (Promega). The presence of alkaline phosphatase was detected using the one-step nitroblue tetrazolium–5-bromo-4-chloro-3-indolylphosphate (NBT-BCIP) system (Pierce, Rockford, IL).

Affinity purification and MS. Affinity purification, mass spectrometry (MS) sample preparation, MS analysis, and protein database searches for PLRV were performed as outlined previously (59, 69). Locally infected *N. benthamiana* tissue was homogenized and PLRV (virions and structural proteins) enriched for by affinity purification. Captured proteins were subjected to tryptic digestion and peptides analyzed using an Orbitrap Fusion Tribrid mass spectrometer (Thermo Scientific). Accurate mass measurements on the peptide precursor ions were obtained in the Orbitrap mass analyzer, while peptide fragmentation for sequence identification was produced using collision-induced dissociation in the linear ion trap. The resulting tandem mass spectra were used for protein identification and searched against an in-house protein database of amino acid sequences corresponding to all coding gene sequences from *N. benthamiana* and protein sequences from virus species within the *Luteoviridae* obtained from NCBI using the Mascot search engine. In the luteovirid RTP sequences, an X was included at the position of the CP stop codon to represent any amino acid residue. Peptides spanning the CP-RTD junction were initially identified from the resulting Mascot searches using the following criteria: peptides had to have precursor mass measurement errors within 10 ppm, Mascot ions scores $\geq$20, and expected values (E values) less than 0.02. Spectra corresponding to these peptides were manually verified using predicted fragmentation tables generated by the Protein Prospector MS-Product web tool (http://prospector.ucsf.edu).

ACKNOWLEDGMENTS

We are grateful to Washington da Silva and Sarah Ruark from Cornell University for their comments and helpful suggestions on the manuscript, to Jelena Kraft, Iowa State University, for advice on SHAPE probing, and to the reviewers for valuable advice.

This work was supported by grants to S.M.G. from the National Institute of Food and Agriculture (grant number 2011-04037) and NSF Basic Research to Enable Agricultural Development (NSF-BREAD) (grant number 1109989), NIH grant no. 4R01GM067104-12

to W.A.M., NIH grant no. P41 GM103533 to M.J.M., USDA ARS CRIS project 8062-22410-006-00-D to M.H., and a Graduate Minority Assistanceship Program partial tuition scholarship to E.J.C.

REFERENCES

1. Beier H, Grimm M. 2001. Misreading of termination codons in eukaryotes by natural nonsense suppressor tRNAs. Nucleic Acids Res 29:4767–4782. https://doi.org/10.1093/nar/29.23.4767.
2. Dreher TW, Miller WA. 2006. Translational control in positive strand RNA plant viruses. Virology 344:185–197. https://doi.org/10.1016/j.virol.2005.09.031.
3. Firth AE, Brierley I. 2012. Non-canonical translation in RNA viruses. J Gen Virol 93:1385–1409. https://doi.org/10.1099/vir.0.042499-0.
4. Newburn LR, White KA. 2015. Cis-acting RNA elements in positive-strand RNA plant virus genomes. Virology 479–480:434–443.
5. Jungreis I, Lin MF, Spokony R, Chan CS, Negre N, Victorsen A, White KP, Kellis M. 2011. Evidence of abundant stop codon readthrough in Drosophila and other metazoa. Genome Res 21:2096–2113. https://doi.org/10.1101/gr.119974.110.
6. Song H, Mugnier P, Das AK, Webb HM, Evans DR, Tuite MF, Hemmings BA, Barford D. 2000. The crystal structure of human eukaryotic release factor eRF1—mechanism of stop codon recognition and peptidyl-tRNA hydrolysis. Cell 100:311–321. https://doi.org/10.1016/S0092-8674(00)80667-4.
7. Laurberg M, Asahara H, Korostelev A, Zhu J, Trakhanov S, Noller HF. 2008. Structural basis for translation termination on the 70S ribosome. Nature 454:852–857. https://doi.org/10.1038/nature07115.
8. von der Haar T, Tuite MF. 2007. Regulated translational bypass of stop codons in yeast. Trends Microbiol 15:78–86. https://doi.org/10.1016/j.tim.2006.12.002.
9. Harrell L, Melcher U, Atkins JF. 2002. Predominance of six different hexanucleotide recoding signals 3′ of read-through stop codons. Nucleic Acids Res 30:2011–2017. https://doi.org/10.1093/nar/30.9.2011.
10. Firth AE, Wills NM, Gesteland RF, Atkins JF. 2011. Stimulation of stop codon readthrough: frequent presence of an extended 3′ RNA structural element. Nucleic Acids Res 39:6679–6691. https://doi.org/10.1093/nar/gkr224.
11. Brown CM, Dinesh-Kumar SP, Miller WA. 1996. Local and distant sequences are required for efficient readthrough of the barley yellow dwarf virus PAV coat protein gene stop codon. J Virol 70:5884–5892.
12. Miller WA, Jackson J, Feng Y. 2015. Cis- and trans-regulation of luteovirus gene expression by the 3′ end of the viral genome. Virus Res 206:37–45. https://doi.org/10.1016/j.virusres.2015.03.009.
13. Cimino PA, Nicholson BL, Wu B, Xu W, White KA. 2011. Multifaceted regulation of translational readthrough by RNA replication elements in a tombusvirus. PLoS Pathog 7:e1002423. https://doi.org/10.1371/journal.ppat.1002423.
14. Bahner I, Lamb J, Mayo MA, Hay RT. 1990. Expression of the genome of potato leafroll virus: readthrough of the coat protein termination codon in vivo. J Gen Virol 71:2251–2256. https://doi.org/10.1099/0022-1317-71-10-2251.
15. Filichkin SA, Lister RM, McGrath PF, Young MJ. 1994. In vivo expression and mutational analysis of the barley yellow dwarf virus readthrough gene. Virology 205:290–299. https://doi.org/10.1006/viro.1994.1645.
16. Harrison BD. 1999. Steps in the development of luteovirology, p 1–14. *In* Smith HG, Barker H (ed), The Luteoviridae. CABI Publishing, Wallingford, UK.
17. Brault V, van den Heuvel JF, Verbeek M, Ziegler-Graff V, Reutenauer A, Herrbach E, Garaud JC, Guilley H, Richards K, Jonard G. 1995. Aphid transmission of beet western yellows luteovirus requires the minor capsid read-through protein P74. EMBO J 14:650–659.
18. Jolly CA, Mayo MA. 1994. Changes in the amino acid sequence of the coat protein readthrough domain of potato leafroll luteovirus affect the formation of an epitope and aphid transmission. Virology 201:182–185. https://doi.org/10.1006/viro.1994.1283.
19. Wang JY, Chay C, Gildow FE, Gray SM. 1995. Readthrough protein associated with virions of barley yellow dwarf luteovirus and its potential role in regulating the efficiency of aphid transmission. Virology 206:954–962. https://doi.org/10.1006/viro.1995.1018.
20. Chay CA, Gunasinge UB, Dinesh-Kumar SP, Miller WA, Gray SM. 1996. Aphid transmission and systemic plant infection determinants of barley yellow dwarf luteovirus-PAV are contained in the coat protein readthrough domain and 17-kDa protein, respectively. Virology 219:57–65. https://doi.org/10.1006/viro.1996.0222.
21. Guilley H, Wipf-Scheibel C, Richards K, Lecoq H, Jonard G. 1994. Nucleotide sequence of cucurbit aphid-borne yellows luteovirus. Virology 202:1012–1017. https://doi.org/10.1006/viro.1994.1429.
22. Brault V, Mutterer J, Scheidecker D, Simonis MT, Herrbach E, Richards K, Ziegler-Graff V. 2000. Effects of point mutations in the readthrough domain of the beet western yellows virus minor capsid protein on virus accumulation in planta and on transmission by aphids. J Virol 74:1140–1148. https://doi.org/10.1128/JVI.74.3.1140-1148.2000.
23. Hogenhout SA, van der Wilk F, Verbeek M, Goldbach RW, van den Heuvel JF. 2000. Identifying the determinants in the equatorial domain of Buchnera GroEL implicated in binding Potato leafroll virus. J Virol 74:4541–4548. https://doi.org/10.1128/JVI.74.10.4541-4548.2000.
24. van den Heuvel JF, Bruyere A, Hogenhout SA, Ziegler-Graff V, Brault V, Verbeek M, van der Wilk F, Richards K. 1997. The N-terminal region of the luteovirus readthrough domain determines virus binding to Buchnera GroEL and is essential for virus persistence in the aphid. J Virol 71:7258–7265.
25. Peter KA, Gildow F, Palukaitis P, Gray SM. 2009. The C terminus of the polerovirus p5 readthrough domain limits virus infection to the phloem. J Virol 83:5419–5429. https://doi.org/10.1128/JVI.02312-08.
26. Mutterer JD, Stussi-Garaud C, Michler P, Richards KE, Jonard G, Ziegler-Graff V. 1999. Role of the beet western yellows virus readthrough protein in virus movement in *Nicotiana clevelandii*. J Gen Virol 80:2771–2778. https://doi.org/10.1099/0022-1317-80-10-2771.
27. Peter KA, Liang D, Palukaitis P, Gray SM. 2008. Small deletions in the potato leafroll virus readthrough protein affect particle morphology, aphid transmission, virus movement and accumulation. J Gen Virol 89:2037–2045. https://doi.org/10.1099/vir.0.83625-0.
28. Reavy B, Arif M, Cowan GH, Torrance L. 1998. Association of sequences in the coat protein/readthrough domain of potato mop-top virus with transmission by Spongospora subterranea. J Gen Virol 79:2343–2347. https://doi.org/10.1099/0022-1317-79-10-2343.
29. Tamada T, Schmitt C, Saito M, Guilley H, Richards K, Jonard G. 1996. High resolution analysis of the readthrough domain of beet necrotic yellow vein virus readthrough protein: a KTER motif is important for efficient transmission of the virus by *Polymyxa betae*. J Gen Virol 77:1359–1367. https://doi.org/10.1099/0022-1317-77-7-1359.
30. Torrance L, Lukhovitskaya NI, Schepetilnikov MV, Cowan GH, Ziegler A, Savenkov EI. 2009. Unusual long-distance movement strategies of Potato mop-top virus RNAs in *Nicotiana benthamiana*. Mol Plant Microbe Interact 22:381–390. https://doi.org/10.1094/MPMI-22-4-0381.
31. Tacke E, Prufer D, Salamini F, Rohde W. 1990. Characterization of a potato leafroll luteovirus subgenomic RNA: differential expression by internal translation initiation and UAG suppression. J Gen Virol 71:2265–2272. https://doi.org/10.1099/0022-1317-71-10-2265.
32. Blanchet S, Cornu D, Argentini M, Namy O. 2014. New insights into the incorporation of natural suppressor tRNAs at stop codons in *Saccharomyces cerevisiae*. Nucleic Acids Res 42:10061–10072. https://doi.org/10.1093/nar/gku663.
33. Liang D, Gray SM, Kaplan I, Palukaitis P. 2004. Site-directed mutagenesis and generation of chimeric viruses by homologous recombination in yeast to facilitate analysis of plant-virus interactions. Mol Plant Microbe Interact 17:571–576. https://doi.org/10.1094/MPMI.2004.17.6.571.
34. Torrance L. 1992. Analysis of epitopes on potato leafroll virus capsid protein. Virology 191:485–489. https://doi.org/10.1016/0042-6822(92)90216-C.
35. Juszczuk M, Zagorski-Ostoja W, Hulanicka DM. 1997. Studies on the translation mechanism of subgenomic RNA of potato leafroll virus. Acta Biochim Pol 44:69–77.
36. Miller WA, White KA. 2006. Long-distance RNA-RNA interactions in plant virus gene expression and replication. Annu Rev Phytopathol 44:447–467. https://doi.org/10.1146/annurev.phyto.44.070505.143353.
37. Brierley I, Pennell S, Gilbert RJ. 2007. Viral RNA pseudoknots: versatile motifs in gene expression and replication. Nat Rev Microbiol 5:598–610. https://doi.org/10.1038/nrmicro1704.

38. Mortimer SA, Kidwell MA, Doudna JA. 2014. Insights into RNA structure and function from genome-wide studies. Nat Rev Genet 15:469–479. https://doi.org/10.1038/nrg3681.
39. Ding Y, Tang Y, Kwok CK, Zhang Y, Bevilacqua PC, Assmann SM. 2014. In vivo genome-wide profiling of RNA secondary structure reveals novel regulatory features. Nature 505:696–700. https://doi.org/10.1038/nature12756.
40. Keiler KC, Feaga HA. 2014. Resolving nonstop translation complexes is a matter of life or death. J Bacteriol 196:2123–2130. https://doi.org/10.1128/JB.01490-14.
41. Beznoskova P, Wagner S, Jansen ME, von der Haar T, Valasek LS. 2015. Translation initiation factor eIF3 promotes programmed stop codon readthrough. Nucleic Acids Res 43:5099–5111. https://doi.org/10.1093/nar/gkv421.
42. Simon AE, Miller WA. 2013. 3′ cap-independent translation enhancers of plant viruses. Annu Rev Microbiol 67:21–42. https://doi.org/10.1146/annurev-micro-092412-155609.
43. Newburn LR, White KA. 2017. Atypical RNA elements modulate translational readthrough in Tobacco necrosis virus-D. J Virol 91:e02443-16. https://doi.org/10.1128/JVI.02443-16.
44. Grimm M, Nass A, Schull C, Beier H. 1998. Nucleotide sequences and functional characterization of two tobacco UAG suppressor tRNA(Gln) isoacceptors and their genes. Plant Mol Biol 38:689–697. https://doi.org/10.1023/A:1006068303683.
45. Zhang J, Ieong KW, Johansson M, Ehrenberg M. 2015. Accuracy of initial codon selection by aminoacyl-tRNAs on the mRNA-programmed bacterial ribosome. Proc Natl Acad Sci U S A 112:9602–9607. https://doi.org/10.1073/pnas.1506823112.
46. Zhang J, Ieong KW, Mellenius H, Ehrenberg M. 2016. Proofreading neutralizes potential error hotspots in genetic code translation by transfer RNAs. RNA 22:896–904. https://doi.org/10.1261/rna.055632.115.
47. Gross T, Siepmann A, Sturm D, Windgassen M, Scarcelli JJ, Seedorf M, Cole CN, Krebber H. 2007. The DEAD-box RNA helicase Dbp5 functions in translation termination. Science 315:646–649. https://doi.org/10.1126/science.1134641.
48. Orlova M, Yueh A, Leung J, Goff SP. 2003. Reverse transcriptase of Moloney murine leukemia virus binds to eukaryotic release factor 1 to modulate suppression of translational termination. Cell 115:319–331. https://doi.org/10.1016/S0092-8674(03)00805-5.
49. Le Roy F, Salehzada T, Bisbal C, Dougherty JP, Peltz SW. 2005. A newly discovered function for RNase L in regulating translation termination. Nat Struct Mol Biol 12:505–512. https://doi.org/10.1038/nsmb944.
50. Takyar S, Hickerson RP, Noller HF. 2005. mRNA helicase activity of the ribosome. Cell 120:49–58. https://doi.org/10.1016/j.cell.2004.11.042.
51. Qu X, Wen JD, Lancaster L, Noller HF, Bustamante C, Tinoco I, Jr. 2011. The ribosome uses two active mechanisms to unwind messenger RNA during translation. Nature 475:118–121. https://doi.org/10.1038/nature10126.
52. Gray S, Cilia M, Ghanim M. 2014. Circulative, "nonpropagative" virus transmission: an orchestra of virus-, insect-, and plant-derived instruments. Adv Virus Res 89:141–199. https://doi.org/10.1016/B978-0-12-800172-1.00004-5.
53. Liu S, Sivakumar S, Wang Z, Bonning BC, Miller WA. 2009. The readthrough domain of pea enation mosaic virus coat protein is not essential for virus stability in the hemolymph of the pea aphid. Arch Virol 154:469–479. https://doi.org/10.1007/s00705-009-0327-7.
54. Blanc S, Drucker M, Uzest M. 2014. Localizing viruses in their insect vectors. Annu Rev Phytopathol 52:403–425. https://doi.org/10.1146/annurev-phyto-102313-045920.
55. Hipper C, Brault V, Ziegler-Graff V, Revers F. 2013. Viral and cellular factors involved in phloem transport of plant viruses. Front Plant Sci 4:154. https://doi.org/10.3389/fpls.2013.00154.
56. Rodrigo G, Zwart MP, Elena SF. 2014. Onset of virus systemic infection in plants is determined by speed of cell-to-cell movement and number of primary infection foci. J R Soc Interface 11:20140555. https://doi.org/10.1098/rsif.2014.0555.
57. Gietz RD, Schiestl RH. 2007. High-efficiency yeast transformation using the LiAc/SS carrier DNA/PEG method. Nat Protoc 2:31–34. https://doi.org/10.1038/nprot.2007.13.
58. Xu Y, Zhou X. 2012. Role of Rice stripe virus NSvc4 in cell-to-cell movement and symptom development in *Nicotiana benthamiana*. Front Plant Sci 3:269. https://doi.org/10.3389/fpls.2012.00269.
59. DeBlasio SL, Johnson R, Mahoney J, Karasev A, Gray SM, MacCoss MJ, Cilia M. 2015. Insights into the polerovirus-plant interactome revealed by coimmunoprecipitation and mass spectrometry. Mol Plant Microbe Interact 28:467–481. https://doi.org/10.1094/MPMI-11-14-0363-R.
60. Wang ZH, Treder K, Miller WA. 2009. Structure of a viral cap-independent translation element that functions via high affinity binding to the eIF4E subunit of eIF4F. J Biol Chem 284:14189–14202. https://doi.org/10.1074/jbc.M808841200.
61. Chenna R, Sugawara H, Koike T, Lopez R, Gibson TJ, Higgins DG, Thompson JD. 2003. Multiple sequence alignment with the Clustal series of programs. Nucleic Acids Res 31:3497–3500. https://doi.org/10.1093/nar/gkg500.
62. Gruber AR, Lorenz R, Bernhart SH, Neubock R, Hofacker IL. 2008. The Vienna RNA websuite. Nucleic Acids Res 36:W70–W74. https://doi.org/10.1093/nar/gkn188.
63. Zuker M. 2003. Mfold web server for nucleic acid folding and hybridization prediction. Nucleic Acids Res 31:3406–3415. https://doi.org/10.1093/nar/gkg595.
64. Kraft JJ, Treder K, Peterson MS, Miller WA. 2013. Cation-dependent folding of 3′ cap-independent translation elements facilitates interaction of a 17-nucleotide conserved sequence with eIF4G. Nucleic Acids Res 41:3398–3413. https://doi.org/10.1093/nar/gkt026.
65. Miras M, Sempere R, Kraft J, Miller W, Aranda M, Truniger V. 2015. Determination of the secondary structure of an RNA fragment in solution: Selective 2′-hydroxyl acylation analyzed by primer extension assay (SHAPE). Bio-Protocol 5:e1386. https://doi.org/10.21769/BioProtoc.1386.
66. Das R, Laederach A, Pearlman SM, Herschlag D, Altman RB. 2005. SAFA: semi-automated footprinting analysis software for high-throughput quantification of nucleic acid footprinting experiments. RNA 11:344–354. https://doi.org/10.1261/rna.7214405.
67. Deigan KE, Li TW, Mathews DH, Weeks KM. 2009. Accurate SHAPE-directed RNA structure determination. Proc Natl Acad Sci U S A 106:97–102. https://doi.org/10.1073/pnas.0806929106.
68. Lee L, Kaplan IB, Ripoll DR, Liang D, Palukaitis P, Gray SM. 2005. A surface loop of the potato leafroll virus coat protein is involved in virion assembly, systemic movement, and aphid transmission. J Virol 79:1207–1214. https://doi.org/10.1128/JVI.79.2.1207-1214.2005.
69. DeBlasio SL, Chavez JD, Alexander MM, Ramsey J, Eng Mahoney JKJ, Gray SM, Bruce JE, Cilia M. 2016. Visualization of host-polerovirus interaction topologies using protein interaction reporter technology. J Virol 90:1973–1987. https://doi.org/10.1128/JVI.01706-15.